Monthly Notices
of the Royal Astronomical Society

Tidal Dissipation in Satellites Interrupts Orbital Expansion and Prevents Hill Sphere Escape

Journal:	*Monthly Notices of the Royal Astronomical Society*
Manuscript ID	MN-22-4991-MJ
Manuscript type:	Main Journal
Date Submitted by the Author:	16-Dec-2022
Complete List of Authors:	Kisare, Andrew; University of Chicago Division of the Physical Sciences, Department of Astronomy and Astrophysics Fabrycky, Daniel ; University of Chicago Division of the Physical Sciences, Department of Astronomy and Astrophysics; The University of Chicago
Keywords:	planets and satellites: dynamical evolution and stability < Planetary Systems, exoplanets < Planetary Systems

MNRAS 000, 1–7 (2022) Preprint 16 December 2022 Compiled using MNRAS LATEX style file v3.0

Tidal Dissipation in Satellites Interrupts Orbital Expansion and Prevents Hill Sphere Escape

A. M. Kisare*, D. C. Fabrycky
Dept. of Astronomy & Astrophysics, University of Chicago, 5640 S. Ellis Ave., Chicago, IL 60637

Accepted XXX. Received YYY; in original form 16 Dec 2022

ABSTRACT

The transit method is a promising means to detect exomoons, but few candidates have been identified. For planets close to their stars, the dynamical interaction between a satellite's orbit and the star must be important in their evolution. Satellites spiral out due to the tide raised on their planet, and it has been assumed that they would likely escape the Hill sphere. Here we follow the evolution with a 3-body code that accounts for tidal dissipation within both the planet and the satellite. We show that tidal dissipation in satellites often keeps them bound to their planet, making exomoons more observable than previously thought. The probability of escape depends on the ratio of tidal dissipation constants Q_p/Q_s, and when this ratio exceeds 0.5, escape is usually avoided. Instead, the satellite moves to an equilibrium in which the spin angular momentum of the planet is not transferred into the orbit of the satellite, but instead is transferred into the orbit of the planet around the star. While the planet continues spinning faster than the satellite orbits, the satellite maintains a semi-major axis of ∼0.3 – 0.4 Hill radii. These states are accompanied with modest satellite eccentricity; surprisingly, the greater the dissipation in the satellite relative to the planet, the more eccentric the final state is, up to values of ∼0.2.

Key words: planets and satellites: dynamical evolution and stability – exoplanets

1 INTRODUCTION

Satellites of planets in the Solar System are common, and the giant planets all host extensive systems of satellites. Their existence, composition, and orbital states have all contributed to theories of the origin of the planets themselves (Peale 1999). With the discovery of more than 5000 exoplanets, it is natural to ask whether those bodies have so-called exomoons.

The most straightforward way to detect exomoons to date involves both the planet and the exomoon transiting in front of the star (Sartoretti & Schneider 1999). Even if the moon itself is not seen transiting, the timing variations it induces on the planet may be seen (Kipping 2009). The first precise transit curves of the first transiting planet were thus searched for exomoons (Brown et al. 2001), starting a cottage industry.

Only a few unverified candidates have been proposed (Kepler-1625, Teachey et al. 2018; Kepler-1708, Kipping et al. 2022). The community has pushed back against the first of those detections (Heller et al. 2019; Kreidberg et al. 2019) despite refined analyses (Teachey & Kipping 2018; Teachey et al. 2020). Other groups proposing candidates based on transit timing (Fox & Wiegert 2021), have also received constructive criticism (Kipping 2020).

With a lack of any definitive detections so far, theory becomes more important, both to reexamine what we really expect for the frequency of exomoons, and perhaps to provide some guidance on where the search could be most fruitful going forward. One may even hope to make Popperian predictions, that are susceptible to falsification (Popper & Weiss 1959).

The most immediate reason we expect exomoons is that moons are nearly ubiquitous in the Solar System. But there are theoretical reasons to expect moons around exoplanets may be even more detectable than straight analogies to the Solar System satellites (Hamers & Portegies Zwart 2018; Moraes & Vieira Neto 2020). Since satellite formation has numerous steps, it is hard to develop confident predictions.

Many have done tidal calculations for moons in the solar system and hypothetical moons around exoplanets. Once a moon has formed, Barnes & O'Brien (2002) articulated that tidal evolution may make the satellite escape from the planet. In fact, Counselman (1973) had already speculated that this type of evolution may have removed primordial moons from Mercury and Venus. Cassidy et al. (2009) looked at the problem even closer, to see how the tidal response of the moon might change the dynamics; we will pick up the theoretical story there, hoping that our theoretical predictions may precede the observations.

The Hill sphere is the region around a planet where the gravity of a planet dominates the motion of test particles (and real moons, to a good approximation). Its size is:

$$r_H = a_p \left(\frac{m_p}{3m_*}\right)^{1/3}, \quad (1)$$

where a is the planet's semi-major axis and m_p and m_* are the mass of the planet and star, respectively. At this distance from the planet lie the Lagrange L_1 and L_2 equilibrium points. These are unstable equilibria though, and a natural satellite placed at them would eventually fall

* E-mail: akisare@uchicago.edu

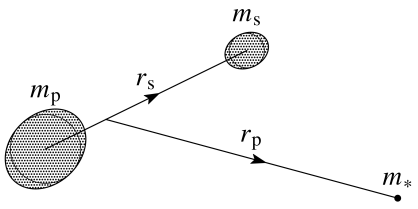

Figure 1. Model components. Tidally distorted and shifted planet and satellite, with a point-mass star referred to the centre of mass of the inner system.

either into heliocentric or into planetocentric orbits. This radius limits of motion of a satellite, but stable motion does not usually extend to that distance. Rather, prograde orbits have $0.5r_H$ as a typical distance (Shen & Tremaine 2008), and orbits initialised further are able to escape beyond L_1 and L_2. The evection resonance, in which the precessional period of the moon equals the planet's orbit around the star, is thought to be the mechanism that finally disrupts a satellite orbit (Grishin et al. 2017). The Coriolis effect makes retrograde satellites more stable than prograde ones (Innanen 1980). Though contained within a zero-velocity curve, stable orbits can quickly transition between circular and eccentric (Hamilton & Burns 1991). These works did not include tides, so we suspected these orbits with fluctuating eccentricities may evolve due to dissipation. We set out to find the outcome.

In the following sections, we describe our numerical methods (§ 2), display the results of individual runs and a suite of runs (§ 3), and describe how the results affect the big picture of exomoon evolution and even detection (§ 4).

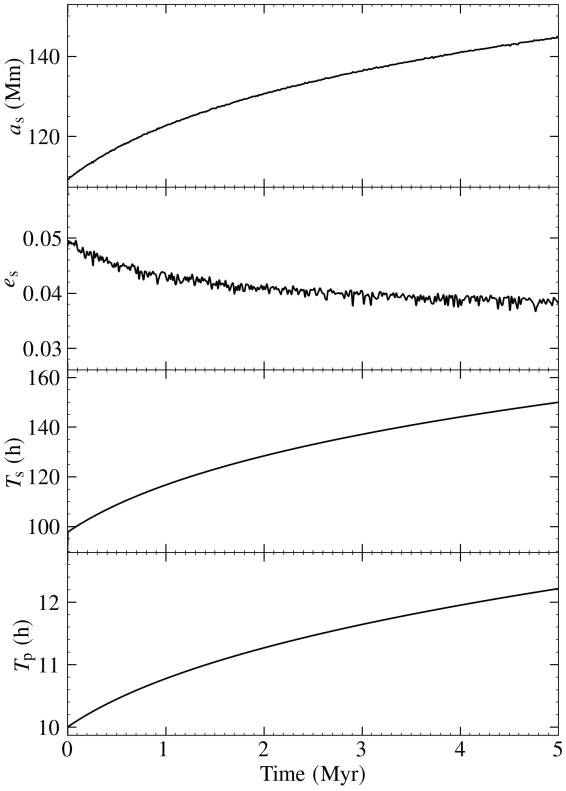

Figure 2. Run 1, with $a_p = 1$ AU. See Table 1 for list of initial conditions.

2 METHODS

Our method involves direct N-body simulations, using the "direct code" of Mardling & Lin (2002).

The hierarchical coordinate system is illustrated by Figure 1. We often describe the orbital elements of the inner pair as that of the satellite. The orbital elements of the outer orbit are often described as that of the planet. The total angular momentum of the system is given by:

$$\boldsymbol{J} = \mu_{ps}(\boldsymbol{r}_p \times \dot{\boldsymbol{r}}_p) + \mu_{ps*}(\boldsymbol{r}_s \times \dot{\boldsymbol{r}}_s) + I_p\boldsymbol{\Omega}_p + I_s\boldsymbol{\Omega}_s. \quad (2)$$

where $\boldsymbol{\Omega}_p$ and $\boldsymbol{\Omega}_s$ are the respective spin vectors of the planet and satellite, $\mu_{ps} = m_p m_s/(m_p + m_s)$, and $\mu_{ps*} = m_* m_p m_s/(m_* + m_p + m_s)$. The four terms are, respectively, the orbital angular momentum of the planet around the star $\boldsymbol{L}_{ps*}$, the orbital angular momentum of the satellite around the planet $\boldsymbol{L}_{ps}$, the spin angular momentum of the planet $\boldsymbol{S}_p$, and the spin angular momentum of the satellite $\boldsymbol{S}_s$. The total angular momentum $\boldsymbol{J}$ should be conserved. To test how well the code conserves angular momentum, we ran a simulation (Run 4, Table 1) with a zero-mass star for simplicity. Over a period of 5 Myr, the absolute error of the total angular momentum $|\delta_J|$ grew approximately linearly to $\sim 2 \times 10^{31}$ kg m^2 s^{-1}. The orbital angular momentum L_{ps} grew 14% to 1.75×10^{34} kg m^2 s^{-1}, at the expense of the planet's spin angular momentum S_p, a value much bigger than the numerical error. The only component with a value smaller than the error was the spin angular momentum of the satellite $S_s \sim 10^{30}$ kg m^2 s^{-1}. However, S_s simply depends on its nearly synchronised state, so its value is not compromised by the numerical error.

We limit our explorations to prograde and coplanar moons, with zero-obliquity planets. Previous work has used an analytical approach (Cassidy et al. 2009) to determine how a star perturbs a tidally-evolving satellite. Our numerical approach is able to see new effects, even though the model is kept simple. The star was placed in a low-eccentricity orbit, also for simplicity.

Parameters we varied were semi-major axis of the planet (as to change the scale of the Hill sphere) as well as the Q-factors of the planet and satellite. We use Earth-like planets and Moon-like satellites, as the Moon is known to have moved out most of its orbital distance due to tides, over the history of the Solar System. Table 1 shows the exact parameters used in our runs.

Rather than using Keplerian elements, which were found to be very poor at qualitatively describing the orbits this far out in the Hill sphere, we use $a_s = (r_{max} + r_{min})/2$ and $e = (r_{max} - r_{min})/(2a_s)$. r_{min} and r_{max} were determined by splitting the positional data into 40 equally-sized intervals, calculating the minimum and maximum radial position in each interval and then interpolating between these values using a piece-wise cubic Hermite interpolating polynomial.

In practice, we found that as the satellite approached the Hill sphere and its orbit became chaotic, the code sometimes abruptly began giving nan (not a number) outputs. We assume that this condition corresponds to an escape of the satellite from around the planet, breaking the hierarchically-defined coordinate system.

We have not computed the effect the star's tidal field has on slowing the rotation of either the planet or the satellite. We discuss the limitation of this approximation in § 4.

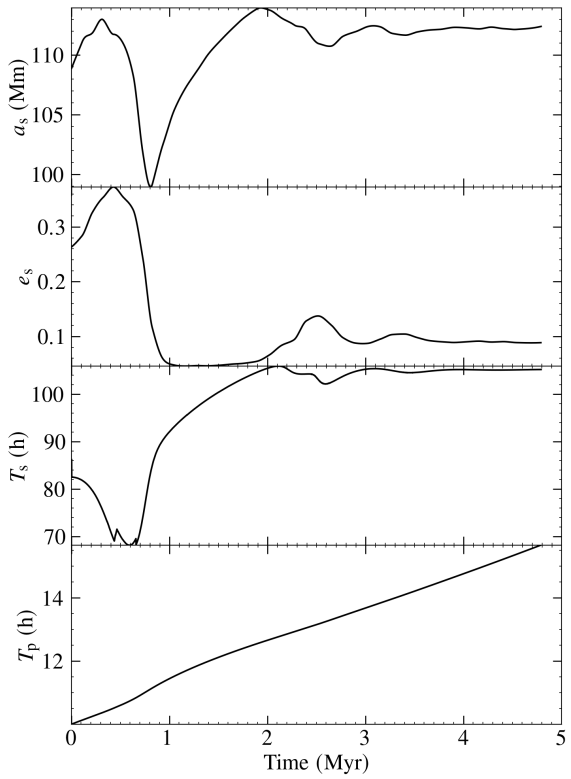

Figure 3. Run 2, with $a_p = 0.18$ AU. See Table 1 for list of initial conditions.

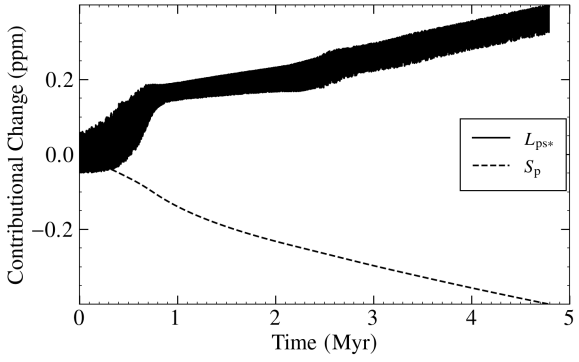

Figure 4. From Run 2, the change in the contribution of the orbital angular momentum of the planet L_{ps*} and the spin angular momentum of the planet S_p to the total angular momentum of the entire system in parts-per-million.

3 RESULTS

First we show the early evolution of the Earth-Moon-Sun system, with the Earth's semi-major axis $a_p = 1$ AU, to give the baseline from which our calculations of close-in planets is an interesting departure (figure 2). We compute just 5 Myr, over which the satellite expands to $\sim 0.1 r_H$ (our Moon is currently at $a_s = 0.25 r_H$, after ~4.5 Gyr of tidal evolution). During this timespan, the Sun does not have a visible effect, beyond the ~0.002 fluctuations in e_s. However, if the star had been much closer, it would have had a large effect. Taking $0.5 r_H$ as the maximum a_s for a stable orbit, this evolution would not be possible beyond $a_s = 112.2$ Mm (at 0.3 Myr) if $a_p = 0.15$ AU or beyond $a_s = 134.7$ Mm (at 2 Myr) for $a_p = 0.18$ AU, and previous authors have assumed the satellite would be stripped at those times. This example motivates the following runs.

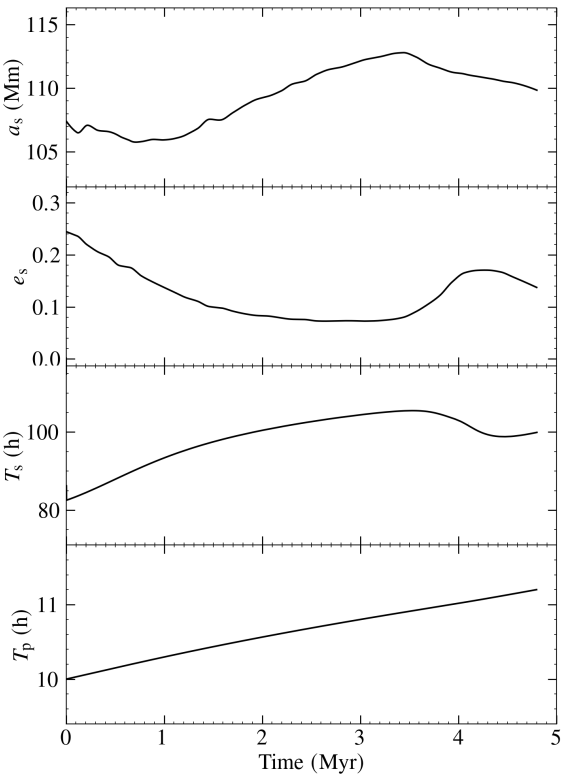

Figure 5. Run 3, see Table 1 for list of initial conditions.

In Figure 3 we show an individual system evolution with $a_p = 0.18$ AU. The satellite approaches the Hill Sphere until approximately 0.3 Myr, after which the satellite is saved from escaping the orbit of the planet and falls back inwards. After 2 Myr, the satellite appears to approach an equilibrium, with a_s consistently varying near 112 Mm ($\sim 0.4 r_H$), with moderate eccentricity and a stable spin period. The spin period of the planet, however, consistently increases during the entire duration of the simulation.

The angular momentum of the planetary spin is thus decreasing, yet the orbit of the moon has stopped evolving. We thus expect that the angular momentum is being transferred to the planetary orbit, i.e. the planet's orbit around the star is growing. Figure 4 illustrates this fact, with the angular momentum of the planet around the star consistently increasing at a similar rate that the spin angular momentum of the planet decreases after the satellite reaches an equilibrium around 3 Myr. To further explore what influences Hill sphere escape, we decided to experiment with two variables: the tidal quality factor of the planet Q_p, and the tidal quality factor of the satellite Q_s.

In Figure 5, we set Q_p larger (Run 3), so that the effect of planetary tides acts over a longer timescale, and the satellite tides have more chance to push the system to the equilibrium. In Run 2 (Figure 3), which has a lower Q_p/Q_s than Run 3, the satellite very quickly approaches the Hill radius, nearly escaping before having a crisis at $t \approx 0.5$ Myr, saving itself, falling back towards the planet, circularizing and reaching an equilibrium. In Run 3, the satellite never dramatically falls inwards before rebounding, and starts its evolution in a state similar to that of Run 2 at ~2.5 Myr.

Running 5817 simulations, each with a unique combination of Q_p and Q_s, we find that runs escape with complicated boundary (Figure 6). We define $\boldsymbol{Q}$ as the vector (Q_s, Q_p) which has a slope Q_p/Q_s and has a magnitude $Q = |\boldsymbol{Q}|$. From this set of simulation data, we organised each data point into 24 bins of slope ranging

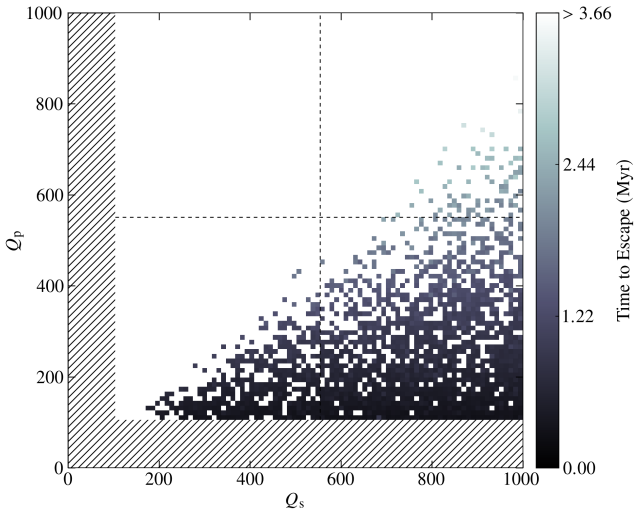

Figure 6. Set of runs showing that both Q_p and Q_s matter for how long the satellite can stay bound to the planet. Each pixel represents a combination of Q_s and Q_p. All the white (empty) pixels had the satellite staying bound to the planet for the full duration of the simulation. The hatched region indicates Q-factors that were not tested. The dotted line demarcates the four separate sets of simulation data that were then stitched together. The upper left quadrant was the most computationally expensive but had the least variation in outcome, so a low resolution of $\Delta Q = 50$/pixel was used there, while the other three quadrants had a resolution of $\Delta Q = (450/43)$/pixel ≈ 10.5/pixel.

from 0.1 to 0.859. For each of these bins, the number of simulations that resulted in an escape of the satellite was divided by the total number of simulations in that bin, giving an escape probability in each bin. Points with $Q > 1000$ were excluded, so as to help balance the number of data points in each bin. This is plotted as the "all Q" histogram in Figure 7a. Two more bins were then created, a "high Q" bin where $743 < Q < 1000$ and a "low Q" bin where $Q \leq 743$. 743 was chosen as the boundary as this value equalises the number of data points in the high Q and low Q bins. The two additional histograms corresponding to these two bins are also plotted in Figure 7a.

We see that there is very little discrepancy between the probability of escape in the high Q region and the low Q region. The sharp drop in probability in the low Q region around $Q_p/Q_s \approx 0.1$, is a consequence of lower slopes being geometrically impossible in this region. The consistency in the escape probability between the high and low regions suggests that escape probability is independent of Q, but is highly dependent on the slope of $\boldsymbol{Q}$, with low slopes yielding higher probabilities of escape, and high slopes yielding probabilities of escape that approach zero. When comparing runs 2 and 3, it can be seen that all else being equal, higher values of Q_p/Q_s reduce the number of opportunities for escape within some time frame, thereby reducing the probability that the satellite does escape, while lower values of Q_p/Q_s give satellites more opportunities to escape within the same time frame, increasing the likelihood of escape.

In Figure 7b, we show that when the satellite did escape, it usually did so faster when Q_p was lower, as expected. Although the relationship is almost linear, there appears to be some curvature in the relationship between Q_p and escape time. Figure 7c suggests that at least some of this curvature is the result of a secondary effect that Q_s has on escape time. For a given value of Q_p, decreasing Q_s seems to have little impact until the very edge between escaping and not escaping, with the escape time sharply increasing at this edge. This effect becomes larger as Q_p increases, resulting in higher values Q_p having much longer escape times than what would otherwise be expected from a linear relationship between Q_p and escape time, as seen in the apparent curvature of Figure 7b. Simply put, dissipation in the planet is the primary determinant of escape time, and dissipation in the satellite opposes escape, having a large impact right at the boundary between escaping and remaining bound to the planet.

One case, at $Q_p = 100$, $Q_s = 686.05$, sticks out as having a lot longer time to escape than its peers. It is an outlier among the points of Figure 7b and Figure 7c, a factor of ~ 3 longer escape time than its peers. It took two shots at escaping, i.e. after the first shot it did not get to a completely stable equilibrium, but took another shot at escaping.

When the satellite does not escape, the satellite moves to a location where it finds an equilibrium getting pushed out by the planet and getting excited to a high enough eccentricity to get pulled in by its own tides at the same rate. This is illustrated by Figure 3. The statistical results at the end of all runs for which the satellite did not escape is shown in Figure 8. Since Q_p controls the speed at which the satellite approaches the Hill Sphere, runs with higher Q_p are less dynamically evolved at the end of the simulation than runs with lower Q_p. This strongly suggests that, in Figure 8a, there is a movement of orbits from the dark-colored region region to the light-colored region. Additionally, Figure 8b shows that even highly evolved orbits (corresponding to the light-colored region of Figure 8a) can stabilise with eccentricity between 0.05 and 0.2 if $log(Q_p/Q_s) > 0$; i.e. $Q_p > Q_s$. Essentially, if the satellite does not escape, systems with strong dissipation in the satellite relative to the planet will stabilise the satellite into a slightly high-eccentricity orbit, whereas systems with weak dissipation in the satellite relative to the planet result in the satellite stabilizing into a more-or-less circular orbit. To us, this result was surprising.

The final state of the system in all these runs is with the planet still out of equilibrium – the planet is spinning down due to tides raised by the satellite on it (Our code does not raise tides on it due to the star, but they would also act to spin down the planet). Future work will look at the even longer-term evolution of the satellite, once the planet has spun down to the satellite's orbital frequency. We expect that from then on, the satellite cannot escape into heliocentric orbit, because the total angular momentum of the planet-satellite system is too low to cause the satellite to reach the Hill sphere. Instead, there would be spin-orbit locking of both the planet and (still) the satellite. Angular momentum would continue to drain at an even slower rate, now due mainly to the tidal bulge the star raises on the planet. This would couple to the satellite's orbit (now the dominant reservoir of angular momentum) and it would very slowly decay.

3.1 Analytic Comparison

Consider the the gravitational "main problem" of lunar theory (Brouwer & Clemence 1961), i.e. just 3 point masses and no rotational or tidal distortion, and no tidal dissipation. If the dominant mass (the star) and the barycentre of the two smaller masses follows a circular orbit, then periodic solutions of these two two smaller masses around each other exist (Henon 1969). The two families of bound, periodic, prograde orbits are called g and g'. Their a_s and e_s (computed as $(r_{max} + r_{min})/2$ and $(r_{max} - r_{min})/2a_s$, respectively) are shown in Figure 9. Family g has low eccentricity, and its nearly-elliptical orbit is a centred ellipse, with long axis forming a right angle with the direction to the star. That is, it makes two radial oscillations for every azimuthal orbit. There is a maximum distance, $0.4297 r_H$, beyond which no similarly shaped orbits are in a steady state. Instead, family g' curves continue to higher a_s at larger e_s, and the figure is no longer centred on the planet but has its long axis

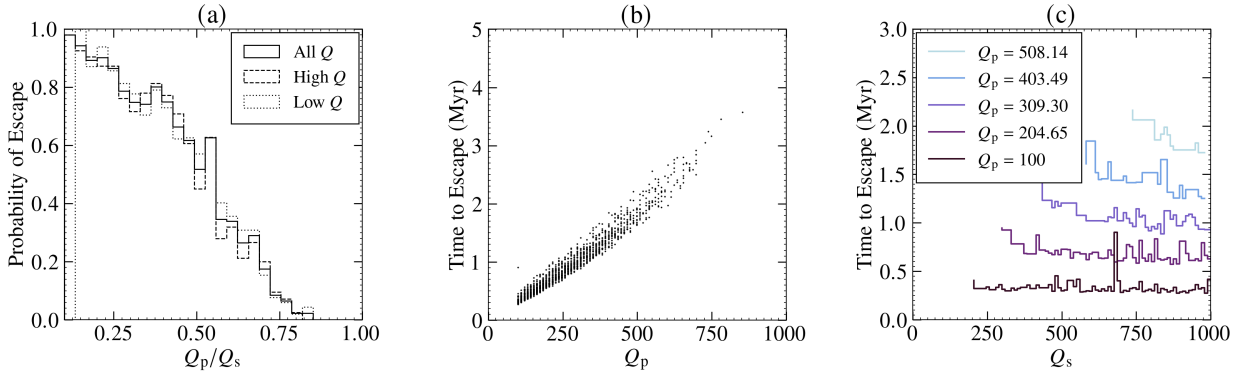

Figure 7. Statistics of Escape: (a) histogram of the probability of escape, versus the Q-ratio Q_p/Q_s, with "high Q" being the region where $743 < Q < 1000$ and "low Q" being the region where $Q \leq 743$; (b) relationship between time to escape and Q_p; (c) effect of Q_s on escape time, for different values of Q_p.

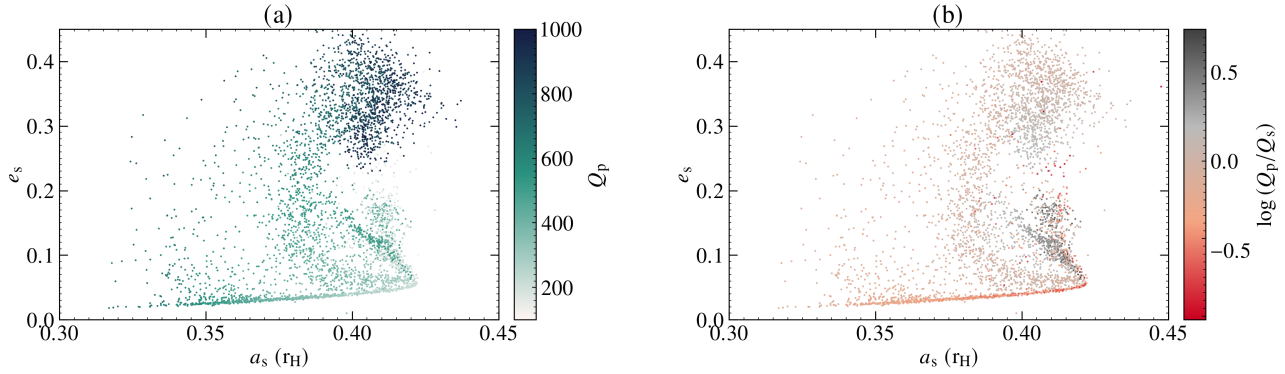

Figure 8. For satellites that did not escape, the final satellite orbits in a/e space: (a) color-bar represents Q_p, controlling how dynamically evolved the system is by the end of the simulation, (b) color-bar represents Q_p/Q_s ratio; strong dissipation in the satellite relative to the planet is gray, whereas weak dissipation in the satellite relative to the planet is red.

pointing either towards or away from the star. That family also ends at $0.704 r_H$.

Our computations actually achieve steady-state figures along family g (fig. 8), when dissipation in the planet dominates that in the satellite (low Q_p/Q_s). For higher values of this ratio, an oscillating orbit obtains, which has an average value of e_s much higher than any of the family g orbits, but also does not extend to as large a_s as family g'.

Prior work on tidal dissipation in planets and satellites have found stable equilibria, limit cycles, and chaotic phases all to be possible states (Meyer & Wisdom 2008). We tentatively identify family g as a possible stable equilibrium actually achievable with only small modification due to rotational and tidal bulges, and dissipation. But the unsteady behavior is a combination of limit cycles (where no escape occurs) and chaotic phases (allowing escape), which is what exists rather than analogies to the steady-state of family g'.

We focus attention on how the system achieves equilibrium on family g. Cassidy et al. (2009) analyzed the problem of the satellite on a variational orbit (family g) and found that tidal dissipation in the satellite could considerably heat — even melt — the satellite. Meanwhile, this energy was coming from the orbit of the star around the planet-moon system, not from the orbit of the moon around the planet. Since the former energy reservoir is enormous, the moon could be heated on timescales of several gigayears with only negligible orbital evolution of the system. However, since the energy does not come at the expense of the moon's orbit, and the tides on

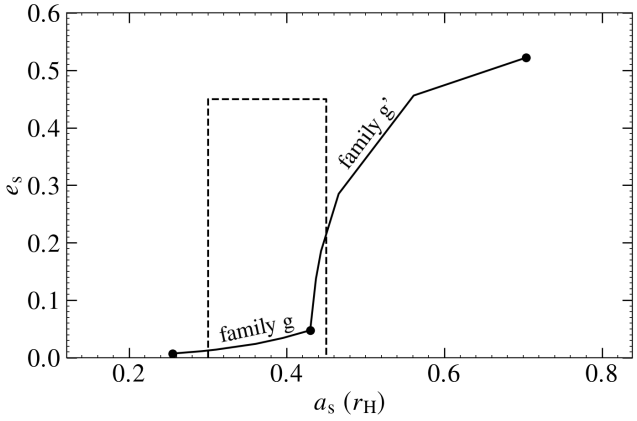

Figure 9. Periodic orbits within Hill's problem, modeling the point-mass 3-body problem in which one of the three masses (the star) is much larger than the other two (Henon 1969). Dashed region corresponds to the boundaries of the plots in figure 8. Dots are transitions between the g and g' families, and the last stable point of the g' family.

the planet continue pumping orbital energy into the moon, this picture does not explain how the moon can reach a steady state in our computation.

We thus sought a higher-order description of the moon's orbit to see how tides could tap the energy of its own orbit. We computed

Table 1. Initial Conditions for Numerical Runs

Parameter	Run 1	Run 2	Run 3[a]	Run 4	Parallel Runs[b]
e_s eccentricity of satellite	0.05	0.05	0.05	0.05	0.05
a_s semi-major axis of satellite (AU)	0.0007277	0.0007277	0.0007277	0.0007277	0.0007277
e_p eccentricity of planet	0	0	0	0	0
a_p semi-major axis of planet (AU)	1	0.18	0.18	0.18	0.18
Inclination of satellite (deg)	0	0	0	0	0
Argument of periapsis of satellite (deg)	0	0	0	0	0
Longitude of nodes of satellite (deg)	0	0	0	0	0
Inclination of planet (deg)	0	0	0	0	0
Argument of periapsis of planet (deg)	0	0	0	0	0
Longitude of nodes of planet (deg)	0	0	0	0	0
m_s mass of satellite (M_L)	1	1	1	1	1
a_p mass of planet ($M_\oplus$)	1	1	1	1	1
m_* mass of Star ($M_\odot$)	1	1	1	0	1
Radius of satellite (R_L)	1	1	1	1	1
Radius of planet ($R_\oplus$).	1	1	1	1	1
T_s spin period of satellite (h)	[c]	[c]	[c]	[c]	[c]
T_p spin period of planet (h)	10	10	10	10	10
Apsidal motion constant of satellite	0.4	0.4	0.4	0.4	0.4
Apsidal motion constant of planet	0.3	0.3	0.3	0.3	0.3
Moment of inertia coefficient of satellite	0.35	0.35	0.35	0.35	0.35
Moment of inertia coefficient of planet	0.3	0.3	0.3	0.3	0.3
Obliquity of satellite	0	0	0	0	0
Obliquity of planet	0	0	0	0	0
Q_s tidal quality factor of satellite	100	100	100	100	100-1000
Q_p tidal quality factor of planet	100	100	403.48	100	100-1000

[a] This run is an element of Parallel Runs
[b] A total of 5817 unique combinations of Q_s and Q_p were simulated.
[c] Synchronised (1:1 and prograde) with the orbit's osculating orbital period, which is not actually an equilibrium due to the strongly perturbed orbit.

the shape of one of the orbits that had achieved this equilibrium, at $a_s = 0.357 r_H$, $e_s = 0.025$. It had a near-180° symmetry in the frame rotating around the planet with the star, with elongation perpendicular to the star's position, like the g-family orbits. The biggest deviation from the perfect g-family orbit was a shift of the satellite's orbit away from the position of the star, by an amount corresponding to an orbital eccentricity around the planet of just 0.00137. This shift is not seen in g-family orbits in Hill's problem, nor in Cassidy et al. (2009)'s analysis, under the approximation of small secondary masses makes the direction towards the star and away from the star completely symmetric.

This small contribution to the orbital shape has one radial excursion per azimuthal orbit, just like normal two-body eccentricity (Kepler's problem). Therefore tidal damping due to that component should indeed result in shrinkage of the satellite's orbit. We conclude that we have found the reason for the steady-state: the orbit deviates slightly from the g family by becoming offset from the planet in the direction away from the star, and this offset generates tidal dissipation which tends to shrink the satellite's orbit, such that it finds an equilibrium with the planetary tide which tends to expand the satellite's orbit.

4 CONCLUSIONS

We have computed the tidal evolution of satellite systems accounting for both tidal dissipation in the planet and in the satellite. If tidal dissipation in an exomoon is comparable or greater than that in their host planet, it can hang out at a substantial fraction of the Hill sphere size, while its host planet's spin rate is decreasing.

In Figure 3 we see that the satellite's orbit comes to an equilibrium in a and e, in which the planet's spin period continues to increase. So the angular momentum must be transferring to the star at a continual rate — an effect was demonstrated in Figure 4 — so the despinning of the planet slightly increases its semi-major axis around the star.

Our calculations have not followed the evolution beyond that point. If the spin rate of the planet keeps decreasing at the same rate as in our calculations (e.g. Run 2) then it will become synchronous with the satellite at $\sim 17(Q_p/100)$ Myr. At this point, the continual perturbations from the star would act to decrease the orbital size, but as the orbit shrinks its rate of angular momentum transfer to the planet's orbit around the star would decrease. But the moon, having avoided escape, would keep the planet spinning above its synchronous rate with respect to the star. The dominant angular momentum transfer would be directly from the spin of the planet to its orbit, based on the direct tide the star raises on the planet, which we have not modelled. That continual leakage of angular momentum from the planet-satellite pair would eventually cause the satellite to be tidally shredded. (Or, it could directly impact the planet, if the planet is much less dense.) After such a shredding episode, the satellite could reconstitute itself as a less massive satellite (Hesselbrock & Minton 2017). At some point the satellite mass would no longer dominate the torque on the planet's spin, and the star would be able to spin-synchronise the planet.

4.1 Application to transiting planets

A typical planet discovered by Kepler has $R_p \sim 1.5 R_\oplus$ and orbits at $a = 0.1$ AU. Depending on whether it is a sub-Neptune or a super-Earth, its Q can be as high as 10^4. Satellites would tend to be smaller (by definition), and perhaps rocky, so their Q would tend to

be lower. Therefore, this mechanism would likely keep the satellite from escaping, and it would keep them at a large separation from the planet ($\sim 0.4 r_{\rm H}$) for hundreds of millions of years.

Currently, the Sun raises about half as big a tide on the Earth in comparison to the Moon, and the degree of dissipation is a function of how fast this bulge moves through the oceans, which is comparable for each because Earth's spin dominates. Therefore, if the Moon were about $2^{1/3} = 1.26$ times further away, (i.e. $0.315 r_{\rm H}$), then the tidal dissipation from the Sun and the Moon would be comparable. At the extreme end of the *g* family, for instance, the Sun's dissipation would be stronger. Our moon would be challenging to detect with even the best photometry (Kipping et al. 2009), so it is more likely to imagine a bigger, more massive satellite that would in fact dominate the tidal despinning of the planet, relative to the star.

Future work could synthesise a population of stars, planets, and moons, at a variety of starting conditions consistent with planet formation, and determine what star-planet separations and planet types would most likely have moons in the tidally-evolved state we have found: low-eccentricity at $\sim 0.4 r_{\rm H}$. We are encouraged that the moon-hunting era is not over with the results of Kepler: we may anticipate moons surviving around planets with periods shorter than the Earth, and hence TESS (Ricker et al. 2015) — and Plato (Rauer et al. 2022) in the future — has a role to play in the hunt for exomoons.

ACKNOWLEDGEMENTS

We thank the Research Computing Center at the University of Chicago for use of the Midway2 cluster, where our runs were completed. Code from Mardling & Lin (2002) was kindly provided by R. Mardling. This work was supported by the University of Chicago Jeff Metcalf Fellowship Grant.

DATA AVAILABILITY

Simulation data may be downloaded at the following DOI: doi/xxx.

REFERENCES

Barnes J. W., O'Brien D. P., 2002, ApJ, 575, 1087
Brouwer D., Clemence G. M., 1961, Methods of celestial mechanics. Academic Press Inc.
Brown T. M., Charbonneau D., Gilliland R. L., Noyes R. W., Burrows A., 2001, ApJ, 552, 699
Cassidy T. A., Mendez R., Arras P., Johnson R. E., Skrutskie M. F., 2009, ApJ, 704, 1341
Counselman Charles C. I., 1973, ApJ, 180, 307
Fox C., Wiegert P., 2021, MNRAS, 501, 2378
Grishin E., Perets H. B., Zenati Y., Michaely E., 2017, MNRAS, 466, 276
Hamers A. S., Portegies Zwart S. F., 2018, ApJ, 869, L27
Hamilton D. P., Burns J. A., 1991, Icarus, 92, 118
Heller R., Rodenbeck K., Bruno G., 2019, A&A, 624, A95
Henon M., 1969, A&A, 1, 223
Hesselbrock A. J., Minton D. A., 2017, Nature Geoscience, 10, 266
Innanen K. A., 1980, AJ, 85, 81
Kipping D. M., 2009, MNRAS, 392, 181
Kipping D., 2020, ApJ, 900, L44
Kipping D. M., Fossey S. J., Campanella G., 2009, MNRAS, 400, 398
Kipping D., et al., 2022, Nature Astronomy, 6, 367
Kreidberg L., Luger R., Bedell M., 2019, ApJ, 877, L15
Mardling R. A., Lin D. N. C., 2002, ApJ, 573, 829
Meyer J., Wisdom J., 2008, Icarus, 193, 213
Moraes R. A., Vieira Neto E., 2020, MNRAS, 495, 3763
Peale S. J., 1999, ARA&A, 37, 533
Popper K. R., Weiss G., 1959, Physics Today, 12, 53
Rauer H., et al., 2022, in European Planetary Science Congress. pp EPSC2022–453, doi:10.5194/epsc2022-453
Ricker G. R., et al., 2015, Journal of Astronomical Telescopes, Instruments, and Systems, 1, 014003
Sartoretti P., Schneider J., 1999, A&AS, 134, 553
Shen Y., Tremaine S., 2008, AJ, 136, 2453
Teachey A., Kipping D. M., 2018, Science Advances, 4, eaav1784
Teachey A., Kipping D. M., Schmitt A. R., 2018, AJ, 155, 36
Teachey A., Kipping D., Burke C. J., Angus R., Howard A. W., 2020, AJ, 159, 142

This paper has been typeset from a TEX/LATEX file prepared by the author.